PROCEEDINGS, Nineteenth Workshop on Geothermal Reservoir Engineering
Stanford University, Stanford, California, January 18-20, 1994
SGP-TR-147

A STUDY OF VAPOR-LIQUID FLOW IN POROUS MEDIA

Cengiz Satik and Yanis C. Yortsos

Petroleum Engineering Program
Department of Chemical Engineering
University of Southern California
Los Angeles, CA 90089-1211

ABSTRACT

We study the heat transfer-driven liquid-to-vapor phase change in single-component systems in porous media by using pore network models and flow visualization experiments. Experiments using glass micromodels were conducted. The flow visualization allowed us to define the rules for the numerical pore network model. A numerical pore network model is developed for vapor-liquid displacement where fluid flow, heat transfer and capillarity are included at the pore level. We examine the growth process at two different boundary conditions.

INTRODUCTION

Vapor-liquid flow in porous media, driven by temperature and pressure gradients, is involved in a wide variety of processes, such as geothermal systems [9, 8, 1], solution gas-drive oil reservoirs [10], thermal oil recovery [5], nuclear waste disposal [3], porous heat pipes [4], boiling [2] and drying [7] These processes share common aspects, such as phase change and its interplay with fluid flow, heat (or mass) transfer and capillarity.

As in other flow processes in porous media, vapor-liquid flows can be described at three different levels: the pore level, where the emphasis is on the mechanisms of nucleation and local interface growth; the pore network level, where the collective action of an ensemble of interacting pores is considered; and the macroscopic or continuum level, where information of the average behavior only is relevant. In the past, the overwhelming majority of theoretical and experimental studies have addressed the continuum level. Continuum approaches make use of Darcy's law extended to multi-phase flow with saturation-dependent relative permeabilities and capillary pressure functions (borrowed from isothermal, immiscible displacement processes) which assume capillary control at the pore level (low Capillary and Bond numbers). These approaches ignore the underlying pore micro structure and require restrictions on scale-dependent viscous and gravity forces. Due to these limitations, continuum approaches may not be fully adequate to describe these vapor-liquid flows. To obtain a better understanding of the process over a very large range of operating conditions, a microscopic approach in which the pore microstructure is acknowledged must be used. A network model approach, in which the porous medium is represented as a two- or three-dimensional network of interconnected simple geometrical shapes of pores (pore bodies or throats), is one such approach that can capture many important details.

To understand key features of heat transfer-driven bubble growth in porous media, we have developed experimental and numerical pore level models. We consider the application of glass micromodels to visualize pore level mechanisms such as nucleation, phase change and phase growth during vapor-liquid flow in porous media.

This paper is organized as follows: First, we discuss our experimental results. Next, we shall describe the numerical pore network model. Finally, we examine its application to two different cases.

EXPERIMENTS

Visualization experiments for boiling and bubble growth in micromodels were carried out to get a better understanding of the phenomena occurring at the microscopic pore level [6].

During one of our visualization experiments, using a microscope, we observed the vapor phase growth in a pore body, following a nucleation event. Shown in Figure 1 are snapshots for the consecutive stages of this event. The time elapsed from the first snapshot to the last is two minutes and ten seconds. Vapor phase first formed on the pore wall at the onset of a nucleation event and it was followed by growth of vapor phase due to the continuous phase change occurring at the liquid-vapor interface. Note that the shape of the microscopic bubble is circular (Figure 1a and b) until it

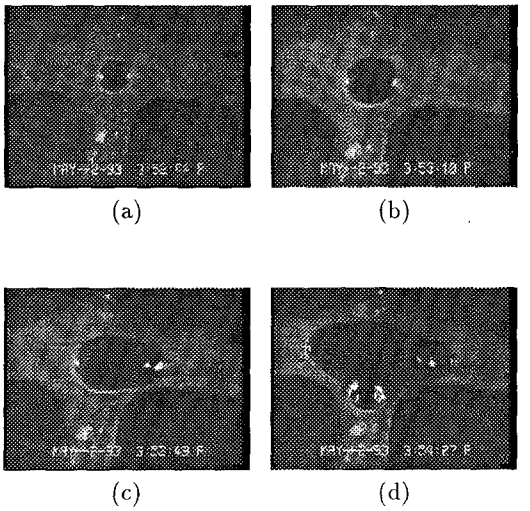

(a) (b) (c) (d)

Figure 1: Observation of vapor phase growth in a pore body, following a nucleation event.

encounters the effects of constraining pore geometry. When this happens, the bubble elongates in the pore body (Figure 1c) and the growth process continues to completely fill the entire pore body (Figure 1d).

Following nucleation, growth of the bubble continues until the pore body is completely filled with vapor phase. When this is completed, bubble cannot grow because of the capillary pressure barrier induced by the constraining pore walls. During this stage, since the volume does not change significantly, the pressure in the vapor phase increases due to the continuous phase change at the liquid-vapor interfaces. We refer this stage as "pressurization step". This stage continues until the capillary pressure barrier is exceeded, which occurs when the difference between the pressures in the vapor and the surrounding liquid phases becomes equal to the capillary pressure. When this condition is achieved, an immediate jump of the interface takes place from one pore body to another. The next stage is a "pore-filling step", during which bubble growth continues until full occupancy is achieved in all pore bodies. During a bubble growth process, these two stages are repeated continuously.

Figure 2 shows a bubble growth pattern obtained during one experiment. As shown in this figure, bubble growth patterns obtained are ramified and not compact, contrary to the growth in the bulk. These patterns reflect the underlying pore microstructure.

PORE NETWORK MODEL

To describe bubble growth in a porous medium, we used a pore network model by representing the

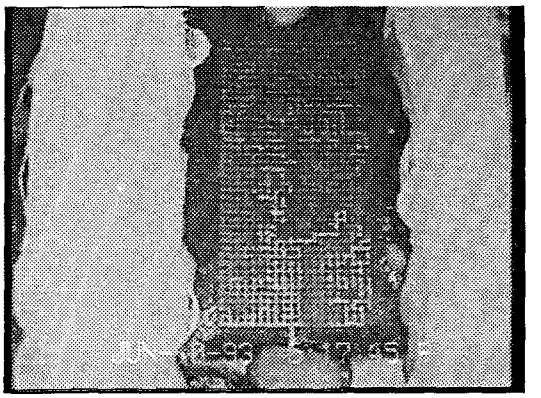

Figure 2: Bubble growth pattern in a horizontal pore network.

porous medium as an equivalent two-dimensional network of interconnected pore bodies and pore throats randomly distributed according to a uniform distribution. We consider growth from a single vapor bubble in a horizontal porous medium of finite size by allowing only one nucleation event to take place at a given location. Details of the model are given in [6]

We examine two different cases: (i) Bubble growth with a uniform superheat imposed initially and (ii) Bubble growth with a prescribed heat flux at one boundary. In the first case, the pore space is completely filled with a superheated liquid. Initial temperatures in the liquid and solid of the porous medium are spatially constant and at the same temperature value. The geometry of the porous medium is square and all four boundaries are open to a constant (atmospheric) pressure. The pressure in the liquid-occupied pore space is initially constant and at atmospheric pressure. In the second case, the geometry of the medium is rectangular. A heat flux is imposed on one side of the medium. No-heat flux boundary conditions are imposed at the remaining boundaries. A constant pressure (atmospheric) boundary condition is imposed on the left-hand side boundary, while no-flux boundary conditions are imposed on all other boundaries of the medium. The initial nucleation site is located at the center of the medium in the first case and at the center of the side where the heat flux is imposed in the second case.

BUBBLE GROWTH IN A UNIFORM INITIAL SUPERHEAT

In the model, we used a square lattice (31x31). Throat (bond) sizes were randomly assigned from a uniform distribution, while pore body (site) sizes were kept constant. Initial temperature and pressure were set to 104.44 °C and 1.0133×10^5 N/m^2,

respectively, and the amount of the superheat imposed was 4.4 °C. Other typical parameters used are shown in Table 1. In the table ρ_l, C_{pl}, λ_l, μ_l, L_v, γ, ρ_v, ρ_s, C_{ps}, λ_s, d^*, d^*_{tf}, M, L_b, R^*_b and R^*_s, are liquid density, specific heat, thermal conductivity and viscosity, latent heat, interfacial tension, vapor density, solid density, specific heat and thermal conductivity, dimensionless parameters for solid-to-liquid and solid-to-thin liquid film heat transfer coupling, molecular weight, bond length, average bond and pore body sizes, respectively.

Fluid distributions at two different stages of bubble growth for the typical parameters given in Table 1 are shown in Figure 3. Corresponding time values for these stages are 2.45 and 7.42 seconds, respectively. Many other simulation results with different parameter values and larger network sizes showed that the time spend to reach the final stage is in fact very small (order of a few seconds), implying that heat transfer driven bubble growth of this type is very fast process. In the Figure, white or black colors represent liquid only or vapor only occupancy, respectively, while gray color denotes partial liquid occupancy. The growth regime for the first stage is of percolation type, during which the two steps (pressurization and pore-filling steps) discussed above follow one another and penetration of single interface occurs at the end of each pressurization step with no further interface penetration until it ends. Both fluid distributions shown in the Figure are at the end of a pore-filling step. Therefore, for the first stage, pore bodies are occupied with either vapor- or liquid-only. However, in a regime other than percolation, penetration of multiple interfaces may occur during both pressurization and pore filling steps, hence some of the pore bodies may be partially liquid-occupied, as shown in Figure 3b.

Table 1: Typical parameter values.

ρ_l	=	960.85 kg/m^3
C_{pl}	=	$4.2092 * 10^3$ J/kg − K
λ_l	=	0.6808 W/m − K
μ_l	=	$2.4799 * 10^{-4}$ N − s/m^2
L_v	=	$2.2568 * 10^6$ J/kg
γ	=	0.0584 N/m
ρ_v	=	0.5886 kg/m^3
ρ_s	=	2082.40 kg/m^3
C_{ps}	=	$8.3732 * 10^2$ J/kg − K
λ_s	=	6.808 W/m − K
d^*	=	1
d^*_{tf}	=	0.01
M	=	18 kmol/kg
L_b	=	1320 μm
R^*_b	=	450 μm
R^*_s	=	601 μm

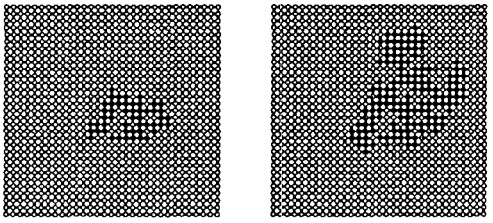

(a) (b)

Figure 3: Fluid distributions at two stages of bubble growth in a uniform initial superheat.

Fluid temperature and pressure and solid temperature distributions corresponding the stages examined above are shown in Figures 4, 5 and 6, respectively. In the Figures, black or white colors denote maximum or minimum values, respectively. As described above, all pore bodies in the network are initially filled with a superheated liquid and initial temperatures in both pore bodies and solid are spatially constant. At the completion of a nucleation event, bubble growth process begins and a liquid-to-vapor temperature gradient forms since the vapor is at the saturation temperature which is lower than the surrounding liquid temperatures. With the existence of such gradient, heat transfer (both conduction and convection) takes place towards the bubble and this drives the phase change process at all liquid-vapor interfaces, resulting to the growth of the bubble. The fluid temperatures in Figure 4 show a good agreement with the above argument. In the Figure, fluid temperatures are constant in the liquid-occupied pore space except in a boundary layer where liquid-to-vapor temperature gradient exist. However, for this particular parameter values, a very sharp gradient is observed.

Solid temperatures, shown in Figure 5, are coupled with liquid temperatures. The measure of coupling between the two fields is provided by a dimensionless parameter d^*. The thermal interaction between solid and liquid increases as d^* increases. We also allow another coupling between the solid and vapor-occupied pore space to account for possible thin liquid films by defining a parameter d^*_{tf}. Solid temperature fields shown in the Figure are almost uniform with maximum and minimum values of 104.44 and 104.39 °C, respectively. Due to the coupling with fluid temperatures, a very small gradient, similar to the liquid-to-vapor temperature gradient in the pore space, is present.

Finally, fluid pressure distributions in Figure 6 shows that the highest pressure is in the bubble while lower pressures are in the liquid indicating the displacement of liquid by vapor. This is expected because the total increase in vapor volume

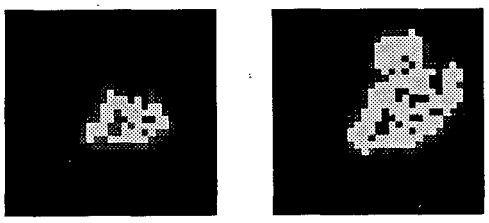

(a) (b)

Figure 4: Fluid temperature distributions at two stages of bubble growth in a uniform initial superheat.

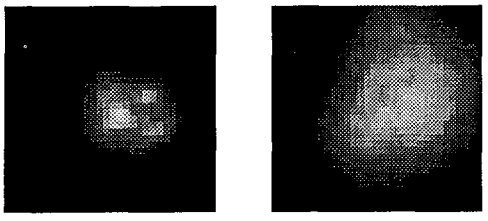

(a) (b)

Figure 5: Solid temperature distributions at two stages of bubble growth in a uniform initial superheat.

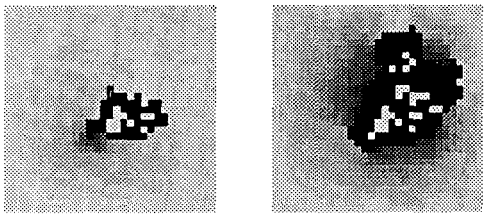

(a) (b)

Figure 6: Fluid pressure distributions at two stages of bubble growth in a uniform initial superheat.

due to phase change is significantly larger than the actual volume of liquid evaporated since the ratio of liquid and vapor densities is very large ($O(10^3)$).

BUBBLE GROWTH WITH A PRESCRIBED HEAT FLUX

To model this process, we used a square lattice (21x42) network with the same bond and site distributions as in the previous case. Now, initial liquid and solid temperatures are the same, while a heat flux (q_h) is imposed over the first column of the network which represents the solid part of the porous medium. Initial liquid temperature and pressure were set to 100 °C and 1.0133×10^5 N/m^2, respectively. The initial nucleation site was arbitrarily located at the node (11,1). Onset of nucleation takes place when the temperature of the node (11,1) reaches the nucleation temperature. Fluid and Solid temperature fields at two different stages of bubble growth for typical parameters given in Table 1 are are shown in Figures 7 and 8. For this particular run, the onset of nucleation took place at 39.673 second and corresponding time values for these stages are 52.99 and 60.80 seconds, respectively. As in the previous case, fast growth dynamics are also observed. The important difference between this and the previous case is the existence of a prescribed heat flux in the solid temperature field. This heat flux generates a temperature gradient along the solid body of the porous medium, while another gradient also forms in the fluid since both are coupled (Figures 7 and 8). As a result, the liquid phase in the pore spaces become superheated, providing a driving force for bubble growth. The magnitude of the superheat increases as the heat flux is imposed. As in the previous case, liquid-to-vapor gradient also exist in the liquid temperatures since it is a requirement for the bubble growth process. Fluid pressure fields are similar to the ones obtained in the previous case.

CONCLUSIONS

In this paper, we discussed the visualization of boiling and bubble growth in pore networks and presented a pore network model that describes bubble growth in porous media due to a temperature supersaturation. Visualization experiments for boiling in horizontal glass micromodels were conducted. We observed the growth of a micro-

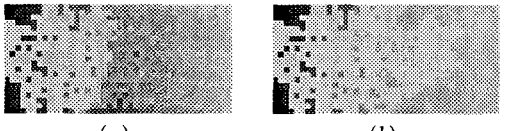

(a) (b)

Figure 7: Fluid temperature fields at two stages of bubble growth with a prescribed heat flux.

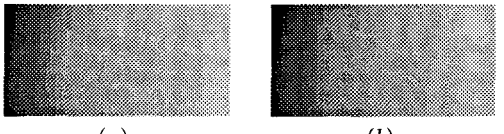

(a) (b)

Figure 8: Solid temperature fields at two stages of bubble growth with a prescribed heat flux.

scopic bubble formed at the onset of a nucleation event. We found that, during bubble growth process, two stages are repeatedly followed: pore-filling and pressurization stages. During the pore-filling stage, the vapor phase is filling a pore body while the liquid is being discharged. During the pressurization stage, the occupancy of all vapor-occupied pore bodies is complete and bubble volume does not change significantly due to the capillary pressure barrier, thus the mass generated at the liquid-vapor interfaces due to the phase change increases the vapor pressure until the capillary pressure barrier is exceeded. When this condition is achieved, a sudden jump of the interface occurs. Contrary to the growth in the bulk, bubble growth patterns in pore networks are ramified and not compact.

The numerical model accounts for fluid flow, heat transfer and capillarity. We have analyzed two different types of bubble growth: (i) Bubble growth with a uniform superheat initially imposed, and (ii) Bubble growth with a constant heat flux imposed. In both cases, the final stages of the growth are reached at very small time values (order of a few second), indicating fast growth. During the bubble growth process, a liquid-to-vapor temperature gradient exist in the fluid temperature fields and this gradient drives the growth. Due to the coupling between liquid and solid temperatures, a similar gradient also exists in the solid temperature fields.

ACKNOWLEDGEMENTS

This work was partly supported by DOE contract DE-FG22-90BC14600, the contribution of which is gratefully acknowledged.

References

[1] N.E. Bixler and C.R. Carrigan. Enhanced heat transfer in partiallly-saturated hydrothermal systems. *Geophysical Res. Letters*, 13:42–45, 1986.

[2] K. Cornwell, B.G. Nair, and T.D. Patten. Observation of boiling in porous media. *J. Heat Mass Transfer*, 19:236–238, 1976.

[3] C. Doughty and K. Pruess. A semianalytical solution for heat-pipe effects near high-level nuclear waste packages burried in partially saturated geological media. *Int. J. Heat Mass Transfer*, 31:79–90, 1988.

[4] Y. Ogniewicz and C.L. Tien. Porous heat pipe. in *Heat Transfer, Thermal Control and Heat Pipes*,(Edited by W.B. Olstad), 70, Progress in Astronautics (Series Editor M. Summerfield) 329-345, AIAA, New York. Presented as paper 79-1093, AIAA 14th Thermophysics Conf., Orlando, Florida, June 1979.

[5] M. Prats. *Thermal Recovery.* SPE Monograph, Dallas, Texas, 1982.

[6] C. Satik. Studies in vapor-liquid flow in porous media. Ph. D. Thesis, May 1994, University of Southern California, Los Angeles, California.

[7] T.M. Shaw. Drying as an immiscible displacement with fluid counterflow. *Phys. Rev. Lett.*, 59:1671, 1987.

[8] C.H. Sondergeld and L. Turcotte. An experimental study of two phase convection in a porous medium with application to geological problems. *J. Geophys. Res.*, 82:2045–2053, 1977.

[9] D.E. White, L.J. Muffler, and A.H. Truesdell. Vapor-dominated hydrothermal systems compared with hot-water systems. *Econ. Geol.*, 66(1):75–97, 1971.

[10] Y.C. Yortsos and M. Parlar. Phase change in porous media: Application to solution gas drive. Paper SPE 19697 presented at the 64th Annual Technical Conf. and Exhibition of SPE, San Antonio, Texas,Oct. 8-11, 1989.